

Size-induced undercooling and overheating in phase transitions in bare and embedded clusters

Chang Q. Sun,^{1,*} Yong Shi,² C. M. Li,³ S. Li,⁴ and T. C. Au Yeung¹

¹*School of Electrical and Electronic Engineering, Nanyang Technological University, Singapore 639798*

²*East Campus, Tangshan University, Hebei Province, China 063020*

³*School of Chemical and Biomedical Engineering, Nanyang Technological University, Singapore 639798*

⁴*School of Materials Science and Engineering, University of New South Wales, Sydney NSW2052, Australia*

(Received 20 September 2005; revised manuscript received 2 December 2005; published 3 February 2006)

The correlation between the thermal stability and electroaffinity of a nanosolid has been explored from the perspective of surface and interface bond-order deficiency. It turns out that the coherency of an atom at the grain boundary and the portion of atoms in the skin of a nanosolid dominate the size dependence of critical temperatures (T_C) for phase transitions. The trapping potential well depression at the surface and interface not only shifts the valence density of state positively but also enlarges the electroaffinity that determines the strength of the bond. In particular, bond-nature alteration at the junction interface, or bond-nature evolution with the reduction of atomic coordination of III- or IV-A atoms, dominates the irregular T_C change with the sizes of the embedded or the III- or IV-A bare nanosolids. Atoms in “superficial” or “interfacial” skins play the core role in dictating the size effect on the thermal stability and electroaffinity of a nanosolid whereas atoms in the core interior remain as they are in the bulk.

DOI: 10.1103/PhysRevB.73.075408

PACS number(s): 81.40.Jj, 36.40.-c

I. INTRODUCTION

Studies of basic phase transitions in nanoscale materials are of great fundamental importance to modern condensed-matter physics. One of the striking features of a nanosolid is that the critical temperatures [$T_C(K_j)$] for phase transitions, such as solid-liquid, liquid-vapor, magnetic-paramagnetic, ferroelectric-paraelectric transitions, are no longer constant but are tunable with size K_j in divergent ways.¹⁻⁴ The parameter $K_j=R_j/d$ is the dimensionless form of size that equals the number of atoms with diameter d lined along the radius R_j of a spherical dot or cross the R_j thickness of a film.

Generally, the $T_C(K_j)$ of a bare nanosolid or a collection of weakly linked nanosolids drops monotonically with size in a K_j^{-1} fashion (known as undercooling).⁵⁻⁹ Increasing evidence of undercooling prefers the following mechanisms for nanosolid melting: (i) liquid-shell nucleation and growth,^{10,11} (ii) liquid-drop formation,¹² (iii) lattice-vibration instability,⁴ (iv) surface-phonon instability,¹³ (v) surface melting,¹⁴ and (vi) surface bond-order loss.¹⁵ For instance, it has been confirmed that a flat or a curved surface melts at temperatures of from 50 (Ref. 16) to 100 K (Ref. 17) lower than the bulk interior. The melting temperature of a Pd nanowire is lower than the bulk value but higher than that of a spherical Pd dot of the same radius.¹⁸ A quasiliquid skin grows from the surface in the radial direction for both cluster and wire. The surface melting is followed by a breakdown of order in the remaining solid core. The melting of an impurity-free vanadium nanosolid proceeds in a stepwise way; i.e., the surface layer of two to three lattice constants thick melts first and then the abrupt overall melting of the entire cluster follows.¹⁷

In contrast, the $T_C(K_j)$ of an embedded or chemically capped nanosolid is often higher than the bulk $T_C(\infty)$, or called overheating, depending on the interfacial conditions.¹⁹ The T_m elevation of the chemically capped nanosolid is attributed to the difference of surface energy between the guest

and host matrix materials.^{12,20,21} It was suggested that overheating would happen if the nanosolid is embedded in a matrix of smaller atoms.²²

However, it is intriguing that the $T_m(K_j)$ of a bare cluster comprising atoms of III- or IV-A element varies nonmonotonically with size. When the solid size is reduced to nanometer scale, the T_m drops with size following the general scaling relation of $T_C(K_j) \propto K_j^{-1}$ (Ref. 1). With a further reduction of the solid size to a scale that contains $n < 60$ atoms, the T_m turns up towards values that are 10%–100% or even higher than the $T_m(\infty)$.²³⁻²⁶ Recent calorimetric measurements²⁷ clarified that the bare Sn_{10-11}^+ clusters can sustain until 1073 K whereas $\text{Sn}_{n>20}^+$ or $\text{Sn}_{n<8}^+$ clusters melt at 670–760 K in comparison to the $T_m(\infty)$ of 505 K. The irregular T_m change of these kinds of nanosolids was attributed either to the bond nature alteration from covalent-metallic to pure covalent with slight bond contraction,²⁴ or to the heavily geometrical reconstruction because Ge, Si, and Sn clusters are found to be stacks of stable tricapped triangular prism units rather than the tetrahedron,²⁸ despite the “magic number” effect.

It is even more intriguing that both the superconductive T_C and the valence density of state (DOS) oscillate when the atomic-layered Pb film is grown on stepped Si substrate.²⁹ The T_C increases gradually with thickness associated with T_C oscillations in layer-by-layer growth. The valence DOS oscillates between zero (for an odd layer with a T_C dip valley) and 0.35 eV (for an even layer with T_C peak) below E_F .³⁰ The oscillation of T_C and the DOS indicates clearly a common origin that governs both the thermal stability and the charge energy of the specimen.

A theoretical approach is yet lacking towards consistent understanding of the divergence in the trends of the size-induced $T_C(K_j)$ change and its correlation to the valence DOS shift. Here we show that such observations could be reconciled in terms of the recently developed bond-order-

length-strength (BOLS) correlation mechanism^{31,32} and its perturbation to the Hamiltonian, atomic coherency, and electroaffinity due to bond-order deficiency of atoms in the surface and interface skins.

II. PRINCIPLES

A. Extended BOLS correlation

According to the BOLS correlation,^{31,32} coordination (CN or z_i) deficiency of an atom denoted i at site surrounding a defect (void, stacking fault, impurity, etc.) or near the surface edge causes the remaining bonds of the undercoordinated atom to contract spontaneously from the bulk value d to the specific d_i , with a coefficient of $c_i(z_i) = d_i/d = 2/\{1 + \exp[(12 - z_i)/(8z_i)]\}$.^{31,32} This spontaneous process is associated with bond strength gain, or trapping potential well depression, from bulk value E_b to E_i ($E_i = c_i^{-m} E_b$). The bond character m being subject to change is intrinsic for a specific material.^{33,34} Consequently, densification and localization of charge, energy, and mass would happen in the surface and interface skins, yet the core interior undergoes little change if no impurity is involved. The depression of the potential well of trapping shifts the energy of the occupied local DOS positively,³¹ which has been identified as “end states” at the end of gold atomic chains on Si substrate,³⁵ and copper atomic chains on Cu(111) surface.³⁶ The trapping potential well depression in the grain boundaries influences significantly the scattering of electrons in thermal³⁷ and electronic conductance³⁸ of small clusters. The atomic cohesive energy or atomic coherency, being the sum of bond energy over all the coordinates, of the specific i th atom will change from the bulk value E_B to E_I by $E_I/E_B = z_i/z_b c_i^{-m} = z_{ib} c_i^{-m}$.

It is important to note that bond contraction also happens at liquid surfaces³⁹ and at sites surrounding atomic voids^{40,41} or substitution impurities.⁴² The spacing between the first and second atomic surface layers of liquid Sn has been measured to contract by 10% relative to that of subsequent layers.³⁹ A substitution doping of Bi and As could induce a 8% contraction of bonds surrounding the As and Bi impurities in a CdTe compound.⁴² The discovery of impurity-induced bond contraction could provide an atomistic understanding of interfacial bond that determines the properties such as mechanical strength in a junction interface such as multilayer structures.^{43,44} The finding of bond contraction at the liquid surface could provide an atomistic mechanism for surface energy. Therefore, the BOLS correlation premise can be extended to the liquid surfaces and junction interfaces. A positive shift of the local DOS is expected at the surface and interface due to the bond-order deficiency induced the potential well depression. With established functional dependence of the detectable quantity on the atomic coherency, electroaffinity, Hamiltonian, or their combinations, one can readily predict the property change of a nanosolid. The BOLS correlation mechanism could be applicable to low-dimensional systems including atomic chains, surface skins, nanograins, defects, junction interfaces, and even amorphous states with randomly distributed atoms with short ordered (bond number loss or bond geometry distortion) bonds.

B. Atomic coherency versus T_C

In principle, the size dependence of a detectable quantity $Q(K_j)$ with atomic-scale density q can be derived according to the core-shell configuration of a nanostructure:^{31,45}

$$\frac{\Delta Q(K_j)}{Q(\infty)} = \begin{cases} \sum_{i \leq 3} \gamma_{ij} \frac{\Delta q_i}{q} = \Delta_q(\tau, K_j) & \text{(BOLS prediction)} \\ B_q/K_j & \text{(measurement)} \end{cases} \quad (1)$$

where $\gamma_{ij} = N_i/N_j = \tau c_i/K_j \leq 1$ is the surface-to-volume ratio with τ being the dimensionality of a spherical dot ($\tau=3$), a rod ($\tau=2$), and a thin slab ($\tau=1$). The subscript i is counted up to 3 from the outermost atomic layer to the center of the solid as no bond-order loss is expected for $i > 3$. The term B_q/K_j is the scaling relation for the measured size dependence with slope B_q being an adjustable parameter. The core-shell configuration favors a recent Editorial note⁴⁶ suggesting that the “superficial skin” could be of core importance in determining the photonic and dielectric properties of a semiconductor quantum dot.

Letting the Q be the cohesive energy $E_{\text{coh}}(N_j) = \sum_{i=1}^j N_i z_i E_i = N_j \langle E_B(K_j) \rangle$ with $q_i = E_i = z_i E_i$ being atomic density for a nanosolid containing N_j atoms within j shells, one can readily obtain the relative change of atomic $E_B(K_j)$:

$$\begin{aligned} \langle E_{\text{coh}}(N_j) \rangle &= N_j z_b E_b + \sum_{i \leq 3} N_i (z_i E_i - z_b E_b) \\ &= N_j E_B(\infty) \left[1 + \sum_{i \leq 3} \gamma_{ij} (z_{ib} c_i^{-m(z_i)} - 1) \right] \end{aligned} \quad (2a)$$

$$\frac{\Delta E_B(\tau, K_j)}{E_B(\infty)} = \sum_{i \leq 3} \gamma_{ij} (z_{ib} c_i^{-m(z_i)} - 1) = \Delta_B(\tau, K_j), \quad (2b)$$

where $E_B(\infty) = z_b E_b$ represents the ideal situation without CN imperfection being considered. The product of $z_{ib} c_i^{-m}$ dominates the perturbation to the cohesive energy, $\Delta_B(\tau, K_j)$, of a nanosolid with a given size and dimensionality (constant γ_{ij} value). For a free surface, $\Delta_B(\tau, K_j) < 0$, if no bond nature (m value) alteration happens; for an intermixing interface, $\Delta_B(\tau, K_j)$ may change depending on the interfacial bond strength. As we noted recently, the $\Delta_B(\tau, K_j)$ may increase if the m value increases when the z_i value is reduced.³⁴

In order to loosen all atoms to a certain extent for a phase transition, one has to weaken all the bonds simultaneously by heating the specimen. This process requires of the thermal energy for each atom a certain portion (f_C^2) of atomic coherency.⁴⁷ Extending the given relation for melting, $T_m(\infty) \propto f_m^2 E_B$,⁴⁸ one can readily obtain the relation $T_C(\tau, K_j) \propto f_C^2 E_B(\tau, K_j)$ with a coefficient f_C being the thermal expansion magnitude of an atom at T_C . At the melting point, the f_m is around 3%–5% of the bulk atomic distance. For other phase transitions, $f_C < f_m$. The f_C may vary from case to case depending on the actual process of the phase transition. Fortunately, one does not need to consider the exact value of f_C if one considers the relative T_C change of a

certain kind of phase transition. Therefore, an analytical expression for the relative change of critical temperatures for possible phase transitions such as evaporation, solid-liquid transition, and magnetic phase transition can be obtained in a universal form

$$\frac{\Delta T_C(\tau, K_j)}{T_C(\infty)} = \frac{\Delta E_B(\tau, K_j)}{E_B(\infty)} = \Delta_B(\tau, K_j) = \Delta'_B \tau / K_j. \quad (3)$$

Equilibrating the predictions with the measurements that follow the scaling relation [see Eq. (1)] for T_m suppression, one can obtain the m value through $\Delta'_B = \sum_{i \leq 3} c_i (z_{ib} c_i^{-m} - 1) = B_q / \tau$. Note that the m value is intrinsic for a specific material and it is independent of the particular property examined. From this perspective, m is not freely adjustable. One may define $\alpha = z_{ib} c_i^{-m}$ as an adjustable quantity to tie up contributions from the involved factors of an interface or a surface (bond nature, bond length, and effective CN). Then the α value will dictate the process of overheating ($\alpha > 1$) or undercooling ($\alpha < 1$). At the junction interface of a capped nanosolid, the α represents the interfacial bond strength as no apparent bond-order loss happens, $z_{ib} \sim 1$. For a bare nanosolid, the only possibility of $\alpha > 1$ is that the m value must increase when the z_i is reduced, provided with the given $c_i(z_i)$ relation.

C. Electroaffinity versus valence DOS shift

The potential well depression and energy densification in the surface skin of a solid will perturb the Hamiltonian that determines the entire band structure and related properties³¹ including electroaffinity ε . The electroaffinity is the separation between the vacuum level, E_0 , and the conduction band edge, which represents the ability of holding the bonding electrons. In comparison, the difference in electronegativity between two elements represents the capability of the more electronegative element catching electrons from the less electronegative one. One specimen with a larger value of ε has a higher tendency to hold the caught electrons more firmly.

Figure 1(a) illustrates the size-induced energy shift of a band denoted c . The enlargement of electroaffinity of the specimen results from the conduction band shift and the band gap expansion (for semiconductors only, which is not shown in the diagram). The affinity change follows the relation

$$\begin{aligned} \Delta \varepsilon(\tau, K_j) &= \Delta E_C(\tau, K_j) - \Delta E_C(\infty) - E_G(\tau, K_j)/2 \\ &= [\Delta E_C(\infty) - E_G(\infty)/2] \Delta_H(\tau, K_j), \end{aligned}$$

$$\Delta_H(\tau, K_j) = \sum_{i \leq 3} \gamma_{ij} (c_i^{-m} - 1) = (\tau / K_j) \sum_{i \leq 3} c_i (c_i^{-m} - 1),$$

where $\Delta_H(\tau, K_j)$ is the Hamiltonian perturbation.³¹ As illustrated in Fig. 1(b), the conduction band edge drops sharply from the $E_C(1)$ value of an isolated atom to a maximum at $E_C(K_j \sim 1.5)$ and then recovers in a K_j^{-1} fashion until the bulk value of $\Delta E_C(\infty)$.³¹ The value of $K_j = 1.5$ corresponds to $z_i = 2$ (Ref. 33), which is the case of a monatomic chain ($\tau = 1$) or an fcc unit cell ($\tau = 3$) containing 13 atoms, for

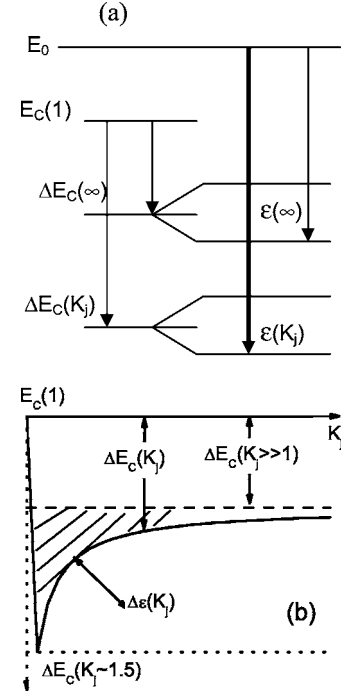


FIG. 1. Correlation between electroaffinity (separation between vacuum level and the conduction band edge) enlargement $\Delta \varepsilon(K_j)$ and conduction band shift $\Delta E_C(K_j)$: $\Delta \varepsilon(K_j) = \Delta E_C(K_j) - \Delta E_C(\infty) - E_G(K_j)/2 - \Delta E_C(\infty) = [\Delta E_C(\infty) - E_G(\infty)/2] \Delta_H$, with Δ_H being the perturbation to the Hamiltonian due to BOLS correlation (Ref. 31). $\Delta E_G(K_j)$ is the size-induced band gap expansion. The energy level drops with the increase of number atoms to the maximum (at $z=2$ for a monatomic chain or a unit cell) and then rises in a K_j^{-1} way to the bulk value, $\Delta E_C(\infty)$. The shaded area corresponds to the electroaffinity enlargement.

instance.^{32,49} Measurements⁵⁰ using x-ray absorption spectroscopy have recently clarified that the occupied Cr- E_{2p} DOS shifts positively by ~ 0.9 eV from the E_{2p} level of an isolated Cr atom, $E_{2p}(1)$, valued at 573.5 eV monotonically to the $E_{2p}(13)$ of 574.4 eV. This finding provides direct evidence for the discussed DOS-affinity relation and the BOLS predicted energy level shift. With the $\Delta E_C(\infty)$ data obtained in Refs. 31, 51, and 52, the maximal $\Delta \varepsilon_M$ value, or the valence DOS shift of the conduction band, of Cu_{3d} [$\Delta E_{3d}(\infty) = 2.12$ eV, $\Delta \varepsilon_M = 0.99$ eV] and Au_{4f} [$\Delta E_{3d}(\infty) = 2.87$ eV, $\Delta \varepsilon_M = 1.34$ eV] nanospheres can be derived using the parameters of $\tau = 3$, $m = 1.0$, and $\Delta_H(1.5) = 0.7^{-1} - 1 = 43\%$. For a semiconductor Si nanosphere ($\tau = 3$ and $m = 4.88$), the electroaffinity will be enlarged by $\Delta_H(1.5) = 0.7^{-4.88} - 1 = 470\%$ of the $\Delta E_{3p}(\infty)$ value. Employing the $\Delta E_{2p}(\infty) = 2.46$ eV and $E_G(\infty) = 1.12$ eV, the estimated $\Delta \varepsilon_M$ for Si is at least 5.8 eV. The actual $\Delta \varepsilon_M$ for Si should be larger as the $\Delta E_{3p}(\infty)$ for the conduction band is larger than the $\Delta E_{2p}(\infty)$.⁵¹ If the m increases with z_i reduction, the $\Delta \varepsilon_M$ is even larger. At a flat surface ($z_i = 4$), the energy level will shift positively by $0.88^{-1} - 1 = 13.6\%$ for metals and $0.88^{-4.88} - 1 = 87\%$ for Si, respectively, as discussed in Ref. 31. The enlarged electroaffinity may further explain why the bond nature alteration happens to the III-A nanosolids and why the IV-A covalent bond becomes even stronger at $z_i \leq 3$ (Ref. 34).

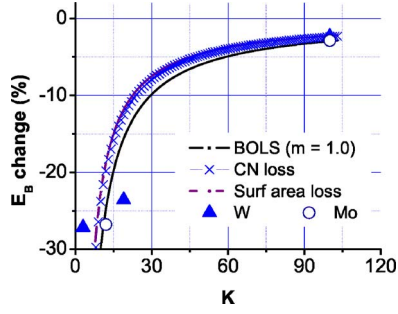


FIG. 2. (Color online) Comparison of the measured size dependence of atomic cohesive energy E_B for Mo and W nanosolids (Ref. 53) with three different models. Numerical agreement is nearly identical for the compared models whereas the physical indications are completely different.

III. RESULTS AND DISCUSSION

In the process of calculation, we used the least-squares linear fit to calibrate the measured data according to the scaling relation given in Eq. (1). This calibration gives rise to the slope B_q and the interception of $Q(\infty)$. We then plotted the predicted curves (for different m and τ values) and the normalized experimental data together for comparison. No precise fitting was necessary as we merely seek for the trend of change and examine the proposed physical origins. Only two typical curves for the slab and spherical dot ($\tau=1$ and 3) were plotted in each panel. For nanosolids with irregular shapes, the normalized data should be located between the two curves. Throughout the course of presentation, we used the dimensionless form of relative change and cluster size K_j . This approach allows us to minimize possible artifacts arising from extrinsic errors (such as instrument system error, temperature fluctuation, or size determination and distribution, and impurity densities). This method also enables us to apply the universal curves to various types of phase transitions and ensures information to be derived purely from the size and interface effects. However, deviation between predictions and measurements should give us information about the possible artificial effects or contributions from other sources. It is necessary to note that the bond character m or its equivalent α parameter in the current approach is intrinsic for a specific material system though the m may be subject to change in the junction interface or with specific elements, as discussed. Using the BOLS premise, one may predict the general trend of property change with an understanding of the nature behind it. The m value or the equivalent α should be subject to some uncertainties (error bars) in the presentation depending on the accuracy of measurement but the accuracy of the m value can be refined by larger sampling volume.

A. E_B and T_C suppression of the bare nanosolids

Figure 2 compares the measured size dependence of atomic cohesive energy $E_B(\tau=3, K_j)$ of Mo and W nanosolids⁵³ with predicted curves given by the following models:

$$\frac{\Delta E_B(\tau, K_j)}{E_B(\infty)} = \begin{cases} \Delta_B(\tau, K_j) & \text{(BOLS correlation)} \\ \sum_{i \leq 3} \gamma'_{ij} [(z_{ib})^{1/2} - 1] & \text{(bond-order loss)} \\ -\beta/K_j & \text{(surface-area loss)} \end{cases}$$

where $\gamma'_{ij} \sim \tau/K_j$ describes situations of bond-order loss without the effect of bond-order-loss-induced bond contraction.⁵⁴ The factor β is an adjustable parameter in the surface-area-loss model.⁵⁵ The former defines the E_B of the i th atom as $E_{B,i} = (z_{ib})^{1/2} E_B(\infty)$; the latter considers the difference between the surface area of the entire particle and the sum of surface areas of all the constituent atoms in isolated state, with the constraint of constant volume before and after solid formation. As can be seen from the figure, at smaller sizes offset shifts become apparent between the compared models. From the viewpoint of numerical calculations, one could hardly tell which model is preferred to others though physical indications of the compared models are entirely different.

Figure 3 compares the predicted with the measured undercooling of nanostructures of (a) Sn and Al on Si_3N_4 substrate,⁵⁶ (b) In⁵⁷ and Pb,⁵⁸ (c) Bi^{56,57} and CdS,⁵⁹ and (d) inert gases of Ne,⁶⁰ Kr,⁶¹ and O nanosolids, and methylchloride (m-CL, only one data point).⁶²

Deviation between prediction and measurement suggests that Al nanosolids grown on SiN substrate are more plate like ($\tau=1, m=1$) throughout the size range of measurement [panel (a)] but Sn-01 [panel (a)] and In-01 and Pb-01 [panel (b)] are more spherical like ($\tau=3$) at particle sizes smaller than 10 nm. However, the indium particle [panel (b)] encapsulated in the controlled-pore silica exhibits slight overheating while the indium embedded in Vycor glass (only one data point) remains undercooling. CdS and Bi nanosolids [panel (c)] exhibit different modes of melting because of the particle-substrate interaction. Deviation also suggests that CdS [panel (c)] and Bi-05 nanosolids are spherical like and other Bi data are scattered between the two curves. The size-dependent T_m of Kr, Ne, and O solids follows the curve of $m=4.88$, despite the accuracy of measurement. Panel (d) also compares the predicted curves for $m=4.88$ and $m=1$. The vertical offset between the two sets of curves with different m values is not that significant unless at very small K_j values. Nevertheless, the m value can be refined by enlarging the size of sampling volume or matching changes of more properties of the same nanomaterial. For example, from fitting the size-dependent data of photoluminescence, photon absorbance, dielectric suppression, electron-phonon interaction, and the core-level shift, we have refined the m value of 4.88 for Si nanosolids.³¹

Figure 4(a) shows the T_C suppression for magnetic Ni thin films,⁶³ Fe_2O_3 nanograins,⁶⁴ and ferroelectric $\text{SrB}_2\text{Ta}_2\text{O}_3$ nanostructures.⁶⁵ Figure 4(b) is the T_{vap} suppression for Ag and PbS nanoparticle evaporation.⁶⁶ It is encouraging that together with the E_B suppression [see Fig. 2(b)] and the undercooling (Fig. 3), the T_C and T_{vap} suppression follows the same predicted curves given by Eq. (3). A $K_0=3$ offset in

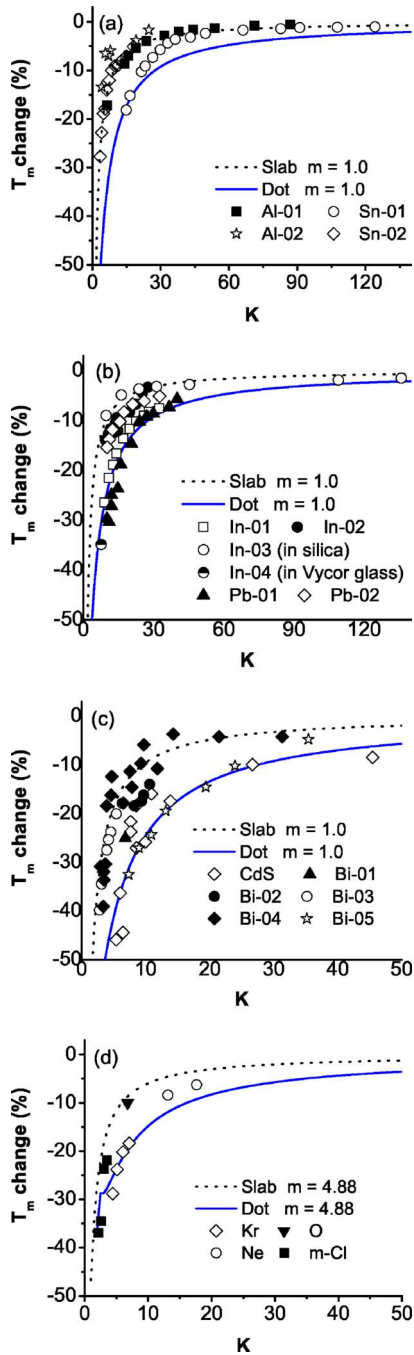


FIG. 3. (Color online) Agreement between predictions (lines) and experimental observations (scattered symbols) of the size and shape dependence of the T_m suppression of (a) Sn and Al on Si_3N_4 substrate (Ref. 56), (b) In (Ref. 57) and Pb (Ref. 58), (c) Bi (Ref. 57) and CdS (Ref. 59), (d) Ne (Ref. 60), Kr (Ref. 61), O, and methylchloride ($m\text{-CL}$, only one data point) (Ref. 62). Al nanosolids grown on SiN substrate are more plate like ($\tau=1$, $m=1$) throughout the sizes of measurement [panel (a)] but Sn-01 on SiN [panel (a)] and In-01 and Pb-01 [panel (b)] are more spherical like ($\tau=3$) at particle size smaller than 10 nm. Indium particles [panel (b)] encapsulated in pore silica matrix are slight overheating compared with Vycor glass matrix. The T_m of Kr, Ne, and O solids follow the curve of $m=4.88$ better despite the accuracy of measurement.

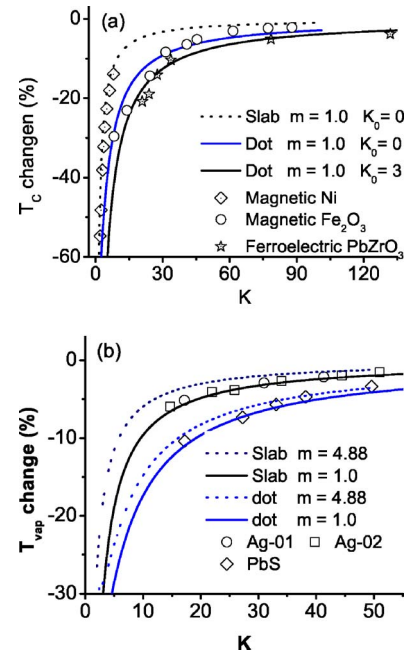


FIG. 4. (Color online) Agreement between BOLS predictions (curves) and measurements (scattered data) of T_c suppression (a) for ferromagnetic Ni films (Ref. 63), and Fe_2O_3 grains (Ref. 64), and ferroelectric SiB_2TaO_3 nanostructures (Ref. 65). The size offset of K_0 represents the contribution from long-order dipole interaction. (b) Liquid-vapor transition (T_{vap}) of Ag and PbS nanosolids (Ref. 66). Agreement gained so far (Figs. 2 and 3) favors the universal trend of the relative change disregarding the actual processes of thermally stimulated phenomena despite the uncertainty being subject to accuracy of measurement.

size for the ferroelectric T_c of $\text{SrB}_2\text{Ta}_2\text{O}_3$ nanograins results from the long-order dipole-dipole interaction that exists widely in the ferroelectric and antiferroelectric materials.⁴⁵

B. Overheating of embedded nanosolids

Figure 5(a) shows the overheating of chemically capped nanosolids. According to Eq (3), overheating of the embedded systems of In/Al ($T_{m,\text{In}}/T_{m,\text{Al}}=530/932$),⁶⁷ Ag/Ni ($1235/1726$),⁶⁸ and Pb/Al ($600/932$) and Pb/Zn ($600/692$)⁶⁹ originates from the interfacial bond strengthening. It is understandable that an atom performs differently at a free surface compared to an atom at the interface. Although the coordination ratio at the interfaces undergoes little change ($z_{ib} \sim 1$), formation of the interfacial compound or alloy alters the nature of the interatomic bond that should be stronger. Energy storage due to bond geometry distortion also contributes to the bond energy. Trends show that overheating happens to substances covered by relatively higher T_m substances, or stronger binding systems, as the T_m relates directly to the atomic coherency. A numerical fit to the measurement leads to a α value of 1.8, indicating that an interfacial bond is 80% stronger than a bond in the bulk of the core material. If we take the bond contraction 0.90–0.92 as determined from the As and Bi doped CdTe compound⁴² into consideration, it is readily found that the m value is around

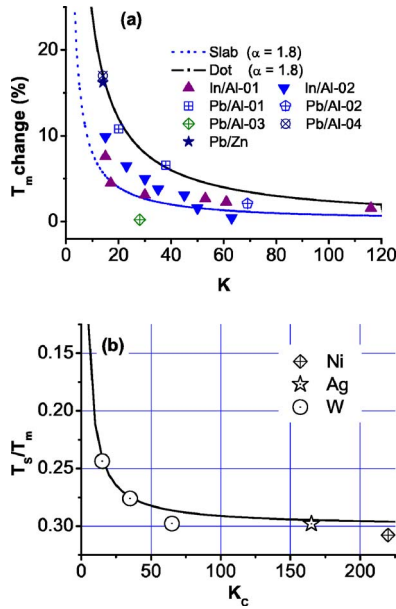


FIG. 5. (Color online) Matching predictions to the measurements of (a) overheating of In (Ref. 67) and Pb (Ref. 69) embedded in Al matrix (Ref. 68), leads to the $\alpha = z_{ib}c_i^{-m}$ values as indicated, which describes the interfacial bond strength. (b) Agreement between BOLS predictions with measurements (Ref. 82) of $T_S = 0.3T_m$ dependence of critical sizes for W [$T_m(\infty) = 3695$ K], Ni (1728 K), and Ag (1235 K) nanocrystal growth.

5.5~7.0. The high m value indicates that the bond nature indeed evolves when a compound is formed. The m value increases from 1 for initially metallic to 4 or higher for the interfacial compound, which indicates the covalent interfacial bond nature. The electroaffinity and the interfacial DOS are expected to shift positively by 80% of the corresponding bulk $\Delta E_C(\infty)$ value. Therefore, the deformed and shortened interfacial bond is much stronger, meaning that electrons at an interface are deeply trapped, giving the interfacial local DOS that could be detectable. From this perspective, twins of nanograins⁷⁰ and the interfaces of multilayered structures⁷¹ should be stronger and thermally more stable.⁴⁴ Interestingly, recent theoretical calculations, confirmed by electron microscopy,⁷² revealed that homojunction dislocations in aluminum could have compact or dissociated core interlayers. The minimum stress required to move an edge dislocation is approximately 20 times higher for compact dislocations than for equivalently dissociated dislocations. As anticipated, this finding provides new insight into the deformation of ultrafine-grained metals and the twin grain boundaries.

C. Nonmonotonic $T_m(K_j)$ change of bare nanosolids

The nonmonotonic T_m change of Sn_n^+ and Ga_n^+ clusters can be simulated by introducing the z_i dependence of the m value at $z_i \leq 3$.³⁴ The T_m curves drop universally with sizes and then turn up at $K_j=3$ (or $z_i=3$). The T_m recovery indicates an essentially higher m value. It is encouraging that a $m(z_i)$ transition from 7 ($z_i=2$) to 1 ($z_i>4$) in the form of $m(z_i) = 1 + 12/\{1 + \exp[(z_i-2)/1.5]\}$ could match closely to the T_m

change of Ga_{17-40}^+ and Sn_{10-500} clusters.³⁴ With the given $c_i(z)$ relation, the m value must increase when the z_i is reduced even though the magic number effect is considered. The stimulated $m(z_i)$ relation indicates a significant enhancement of electroaffinity for the smallest III-A and IV-A elemental clusters. In contrast, the undercoordinated Al-Al surface bond has been found to be shorter ($\sim 5\%$) and stronger with some more covalent characteristics.⁷³⁻⁷⁵ However, the overheating of Al_{49-60}^+ clusters is less significant compared with the heavier III-A Ga_n^+ and the IV-A Sn_n^+ clusters, which might indicate that the m value of the lighter Al atom is less sensitive to the z_i value. Therefore, bond nature alteration with z_i could be unique to the heavier III-A and IV-A atoms.

Understanding may clarify why a small cluster of carbon atoms prefers a ring or a tadpole structure with each atom two bonds²⁵ or tubes and fullerenes with three neighbors rather than the densely packed tetrahedron with four nearest neighbors. The relative cohesive energy for a carbon atom with two, three, and four coordinates can be obtained as $E_I/E_B = z_{ib}c_i^{-2.56} = 0.4195$ ($z_i=2$), 0.4225 ($z_i=3$), and 0.4683 ($z_i=4$). The preference of $z_i=2$ and 3 structures means that the value of $m=2.56$ for a single-wall tube [$z_i=3$ and $m=2.56$ refined by matching the predicted to the observed Young's modulus and melting point change (Ref. 76)] may not hold for $z_i=2$ and 4. The m value of C should also increase when the z_i of a C atom is reduced.

The mechanism of trapping potential well depression and affinity enlargement may provide an alternative understanding of the conductor-insulator transition occurring to the Pd clusters containing 10^{1-2} atoms.⁷⁷ The positive shift of the affinity and conduction DOS and the localization of charges will hinder the charge transport, leading to a manifestation of insulating features of small Pd clusters. Such a conductive-nonconductive transition of clusters at the lower end of the size limit is therefore expected to be common to most elements, in particular for the III-A and IV-A nanosolids because of the size-reduction-enlarged affinity.

The BOLS premise may also present a supplementary understanding to the quantum confinement scheme for the T_C and valence DOS oscillation in the atomic-layered Pb films.²⁹ It has been clear that the T_C drop is related to the atomic coherency change ($z_{ib}c_i^{-m}-1$) whereas the DOS shift depends on the depression of potential well depth ($c_i^{-m}-1$). Generally, the T_C drop is associated with a positive DOS shift. However, if atoms (with $z_i \leq 3$) at islands or at the step edges become dominant, the m value may increase for the IV-A Pb atoms. The m -value increase will result in an upper jump of T_C and a larger DOS shift. This trend is the right case of even Pb layers as observed. Similarly, the association of the T_C dip-drop and valence DOS backshift to E_F may suggest a lower number of such undercoordinates atoms.⁷⁸

D. Temperature dependence of the critical size in nanocrystal growth

The understanding of size-dependent T_C may provide guidelines for growing nanosolids using a sintering method on a heated substrate. For a given temperature of the substrate (T_S), there will be a critical size of the grown particle

in vapor deposition. Any particle larger than the critical size will be deposited as such. On the other hand, if the incident cluster size is smaller than the critical size, the landing particles will melt upon deposition and they will coagulate to produce clusters equal to the critical size or larger. If the T_S is higher than the T_m , the arriving clusters may merge and then evaporate. This intuition implies that the T_S should be as low as possible if one wants to obtain smaller particles. This mechanism also applies to the sinterability of nanosolids. The finding⁷⁹ that the critical size of oxide increases with annealing temperature could evidence for the proposed T_S dependence of the grown particle size. A recent experimental investigation⁸⁰ revealed that the topmost Bi layers on graphite start to lose long-range order at 10–15 K below the Bi bulk melting point, 544.52 K, whereas crystallization occurs from the melt ~ 125 K below $T_m(\infty)$, which shows the temperature difference between melting and solidification of the same surface.

Normally, $T_S(K_j)$ is around 0.3 times $T_m(K_j)$.^{81–83} The T_S dependence of the critical size K_C can be estimated from Eq. (3):

$$T_S(\tau, K_C) = 0.3T_m(\tau, K_j) = 0.3T_m(\infty)(1 + \Delta_B),$$

$$\Delta_B \cong \Delta'_B/K_C,$$

which gives the thermally stable critical size

$$K_C = \frac{-\Delta'_B}{1 - T_S(\tau, K_j)/[0.3T_m(\infty)]} = \frac{\tau \sum_3 c_i (1 - z_{ib} c_i^{-m})}{1 - T_S(\tau, K_j)/[0.3T_m(\infty)]}. \quad (5)$$

It is readily calculated that the constant $\Delta'_B = -2.96$ for a spherical metallic dot ($m=1$, $\tau=3$, $K_C > 3$). The critical size of the deposited nanosolid depends on the ratio of $T_S(\tau, K_j)/[0.3T_m(\infty)]$. The $R_C (=K_C d)$ at T_S can be estimated with the known atomic diameter d and $T_m(\infty)$. Figure 5 shows agreement between the predictions and experimental results.

IV. CONCLUSION

In summary, the extended BOLS correlation premise has enabled us to reconcile divergent trends of the T_C change for various phase transitions of nanoscale materials. The correlation between thermal stability and electroaffinity or valence

DOS shift of nanoscale materials has also been developed in terms of surface and interface atomic CN deficiency. Our understanding may be summarized as follows.

(i) The electroaffinity and valence DOS of a nanoscale specimen shift positively and simultaneously with a reduction of the solid size, which could be observed as “end or edge states” because of the depressed potential well of trapping. The enhanced affinity in the surface and interface skins takes the responsibility for the bond strength gain.

(ii) The thermal stability of a nanosolid is determined by the atomic coherency. The monotonic T_C depression with sizes of the bare nanosolids is dominated by surface bond-order loss while the bond nature or m value remains constant.

(iii) The monotonic T_C elevation of the embedded or chemically capped nanosolids arises from interfacial bond-strength gain due to compound or alloy formation at the junction interface. A deeply trapped interfacial local DOS is anticipated to be associated with larger electroaffinity in the interface skin.

(iv) The nonmonotonic T_C change of the bare III-A and IV-A nanostructures evidences the essentiality of bond nature evolution with atomic coordination reduction of III- or IV-A elements. Results suggest that the irregular T_C change might be unique to the bare III-A and IV-A nanosolids, which offers a challenge for further confirmation with larger sample volume.

(v) It is emphasized that atoms in the “superficial” or “interfacial” skins dominate the performance of a nanosolid whereas atoms in the core interior remain as they are in the bulk counterpart.

(vi) The critical sizes of grown particles can be controlled by adjusting the temperature of the substrate, which should be useful in nanomaterials design.

Understanding of the bond nature alteration of the deformed and shortened bonds at the surface and interface and their correlation to the electroaffinity or DOS shift should inspire efforts towards a consistent understanding of surfaces, interfaces, nanosolids, and atomic-scale defects and their interdependence.

ACKNOWLEDGMENTS

The sabbatical leave of C.Q. at the Institute of Nanotechnology at University of Texas, Dallas, and financial support by Nanyang Technological University, Singapore, under the research program for Bionanosystems are gratefully acknowledged.

*FAX: 65 6792 0415. Electronic address: ecqsun@ntu.edu.sg

¹H. K. Christenson, J. Phys.: Condens. Matter **13**, R95 (2001); J. G. Dash, Rev. Mod. Phys. **71**, 1737 (1999); M. Alcountlabi and G. B. McKenna, J. Phys.: Condens. Matter **17**, R461 (2005).

²V. N. Singh and B. R. Mehta, J. Nanosci. Nanotechnol. **5**, 431 (2005).

³C. C. Yang and Q. Jiang, Acta Mater. **53**, 3305 (2005).

⁴F. G. Shi, J. Mater. Res. **9** 1307 (1994).

⁵M. José-Yacamán, C. Gutierrez-Wing, M. Miki, D.-Q. Yang, K. N. Piyakis, and E. Sacher, J. Phys. Chem. B **109**, 9703 (2005).

⁶R. D. Zysler, D. Fiorani, A. M. Testa, L. Suber, E. Agostinelli, and M. Godinho, Phys. Rev. B **68**, 212408 (2003).

⁷S. Li, T. White, J. Plevart, and C. Q. Sun, Supercond. Sci. Technol. **17**, S589 (2004).

⁸A. V. Pogrebnyakov, J. M. Redwing, J. E. Jones, X. X. Xi, S. Y. Xu, Q. Li, V. Vaithyanathan, and D. G. Schlom, Appl. Phys.

- Lett. **82**, 4319 (2003).
- ⁹S. Bose, P. Raychaudhuri, R. Banerjee, P. Vasa, and P. Ayyub, Phys. Rev. Lett. **95**, 147003 (2005).
- ¹⁰H. Sakai, Surf. Sci. **351**, 285 (1996).
- ¹¹R. R. Vanfleeter and J. M. Mochel, Surf. Sci. **341**, 40 (1995).
- ¹²K. K. Nanda, S. N. Sahu, and S. N. Behera, Phys. Rev. A **66**, 013208 (2002).
- ¹³M. Wautelet, J. Phys. D **24**, 343 (1991).
- ¹⁴B. Wunderlich, Thermochim. Acta **432**, 127 (2005).
- ¹⁵C. Q. Sun, Y. Wang, B. K. Tay, S. Li, H. Huang, and Y. B. Zhang, J. Phys. Chem. B **106**, 10701 (2002).
- ¹⁶S. C. Santucci, A. Goldoni, R. Larciprete, S. Lizzit, M. Bertolo, A. Baraldi, and C. Masciovecchio, Phys. Rev. Lett. **93**, 106105 (2004).
- ¹⁷W. Y. Hu, S. G. Xiao, J. Y. Yang, and Z. Zhang, Eur. Phys. J. B **45**, 547 (2005).
- ¹⁸L. Miao, V. R. Bhethanabotla, and B. Joseph, Phys. Rev. B **72**, 134109 (2005).
- ¹⁹W. Fan and X. G. Gong, Phys. Rev. B **72**, 064121 (2005).
- ²⁰L. H. Liang, C. M. Shen, S. X. Du, W. M. Liu, X. C. Xie, and H. J. Gao, Phys. Rev. B **70**, 205419 (2004).
- ²¹D. Xie, M. P. Wang, and W. H. Qi, J. Phys.: Condens. Matter **16**, L401 (2004).
- ²²Q. Jiang, Z. Zhang, and J. C. Li, Chem. Phys. Lett. **322**, 549 (2000).
- ²³G. A. Breaux, R. C. Benirschke, T. Sugai, B. S. Kinnear, and M. F. Jarrold, Phys. Rev. Lett. **91**, 215508 (2003).
- ²⁴S. Chacko, K. Joshi, and D. G. Kanhere, Phys. Rev. Lett. **92**, 135506 (2004).
- ²⁵Z. Y. Lu, C. Z. Wang, and K. M. Ho, Phys. Rev. B **61**, 2329 (2000).
- ²⁶F. C. Chuang, C. Z. Wang, S. Ogiit, J. R. Chelikowsky, and K. M. Ho, Phys. Rev. B **69**, 165408 (2004).
- ²⁷G. A. Breaux, C. M. Neal, B. Cao, and M. F. Jarrold, Phys. Rev. B **71**, 073410 (2005).
- ²⁸A. A. Shvartsburg, B. Liu, Z. Y. Lu, C. Z. Wang, M. F. Jarrold, and K. M. Ho, Phys. Rev. Lett. **83**, 2167 (1999).
- ²⁹Y. Guo, Y. F. Zhang, X. Y. Bao, T. Z. Han, Z. Tang, L. X. Zhang, W. G. Zhu, E. G. Wang, Q. Niu, Z. Q. Qiu, J. F. Jia, Z. X. Zhao, and Q. K. Xue, Science **306**, 1915 (2004).
- ³⁰Y. F. Zhang, J. F. Jia, T. Z. Han, Z. Tang, Q. T. Shen, Y. Guo, Z. Q. Qiu, and Q. K. Xue, Phys. Rev. Lett. **95**, 096802 (2005).
- ³¹C. Q. Sun, Phys. Rev. B **69**, 045105 (2004).
- ³²C. Q. Sun, C. M. Li, S. Li, and B. K. Tay, Phys. Rev. B **69**, 245402 (2004).
- ³³It has been verified that for pure metals such as Au, Ag, and Ni, $m \equiv 1$ for alloys and for compounds m is around 4 for C and Si. The m has been optimized to be 2.56 and 4.88, respectively.
- ³⁴C. Q. Sun, C. M. Li, H. L. Bai, and E. Y. Jiang, Nanotechnology **16**, 1290 (2005).
- ³⁵J. N. Crain and D. T. Pierce, Science **307**, 703 (2005).
- ³⁶V. S. Stepanyuk, A. N. Klavysyuk, L. Niebergall, and P. Bruno, Phys. Rev. B **72**, 153407 (2005).
- ³⁷T. C. Au Yeung, T. C. Chiam, C. Q. Sun, M. Gu, W. Z. Shangguan, and C. H. Kam, J. Appl. Phys. **98**, 113707 (2005).
- ³⁸T. C. Au Yeung, T. C. Chiam, C. K. Chen, C. Q. Sun, W. Z. Shangguan, W. K. Wong, and C. H. Kam, Phys. Rev. B **72**, 155417 (2005).
- ³⁹O. G. Shpyrko, A. Y. Grigoriev, C. Steimer, P. S. Pershan, B. Lin, M. Meron, T. Graber, J. Gerbhardt, B. Ocko, and M. Deutsch, Phys. Rev. B **70**, 224206 (2004).
- ⁴⁰R. G. Lacerda, M. C. dos Santos, L. R. Tessler, P. Hammer, F. Alvarez, and F. C. Marques, Phys. Rev. B **68**, 054104 (2003).
- ⁴¹C. H. P. Poa, R. G. Lacerda, D. C. Cox, S. R. P. Silva, and F. C. Marques, Appl. Phys. Lett. **81**, 853 (2002).
- ⁴²H. E. Mahnke, H. Haas, E. Holub-Krappe, V. Koteski, N. Novakovic, P. Fochuk, and O. Panchuk, Thin Solid Films **480-481**, 279 (2005).
- ⁴³Z. Shan, E. A. Stach, J. M. K. Wiezorek, J. A. Knapp, D. M. Follstaedt, and S. X. Mao, Science **305**, 654 (2004).
- ⁴⁴Z. Pan, Z. Sun, Z. Xie, L. Hao, S. Wei, J. Xu, and I. Kojima, <http://www.paper.edu.cn/200511-444>
- ⁴⁵C. Q. Sun, W. H. Zhong, S. Li, B. K. Tay, H. L. Bai, and E. Y. Jiang, J. Phys. Chem. B **108**, 1080 (2004).
- ⁴⁶H. Winn, OE Mag. **8**, 10 (2005).
- ⁴⁷X. Y. Qin, X. G. Zhu, S. Gao, L. F. Chi, and J. S. Lee, J. Phys.: Condens. Matter **14**, 2605 (2002).
- ⁴⁸J. Tateno, Solid State Commun. **10**, 61 (1972).
- ⁴⁹The effective CN of a surface atom for a spherical dot follows the relation $z_1=4(1-0.75/K_j)$, and the CN of the subsequent layers are $z_2=6$ and $z_3=12$.
- ⁵⁰M. Reif, L. Glaser, M. Martins, and W. Wurth, Phys. Rev. B **72**, 155405 (2005).
- ⁵¹C. Q. Sun, L. K. Pan, T. P. Chen, X. W. Sun, S. Li, and C. M. Li, Appl. Surf. Sci. **252**, 2101 (2006).
- ⁵²D. Q. Yang and E. Sacher, Appl. Surf. Sci. **195**, 187 (2002).
- ⁵³H. K. Kim, S. H. Huh, J. W. Park, J. W. Jeong, and G. H. Lee, Chem. Phys. Lett. **354**, 165 (2002).
- ⁵⁴D. Tománek, S. Mukherjee, and K. H. Bennemann, Phys. Rev. B **28**, 665 (1983).
- ⁵⁵W. H. Qi and M. P. Wang, J. Mater. Sci. Lett. **21**, 1743 (2002).
- ⁵⁶S. L. Lai, J. R. A. Carlsson, and L. H. Allen, Appl. Phys. Lett. **72**, 1098 (1998); J. Eckert, J. C. Holzer, C. C. Ahn, Z. Fu, and W. L. Johnson, Nanostruct. Mater. **2**, 407 (1993); G. L. Allen, W. W. Gile, and W. A. Jesser, Acta Metall. **28**, 1695 (1980).
- ⁵⁷K. M. Unruh, T. E. Huber, and C. A. Huber, Phys. Rev. B **48**, 9021 (1993).
- ⁵⁸T. B. David, Y. Lereah, G. Deutscher, R. Kofmans, and P. Cheyssac, Philos. Mag. A **71**, 1135 (1995).
- ⁵⁹N. Goldstein, C. M. Echer, and A. P. Alivistos, Science **256**, 1425 (1992).
- ⁶⁰N. Goldstein, Appl. Phys. A: Mater. Sci. Process. **62**, 33 (1996).
- ⁶¹K. Morishige and K. Kawano, J. Phys. Chem. B **104**, 2894 (2000).
- ⁶²E. Molz, A. P. Y. Wong, M. H. W. Chan, and J. R. Beamish, Phys. Rev. B **48**, 5741 (1993).
- ⁶³F. Huang, G. J. Mankey, M. T. Kief, and R. F. Willis, J. Appl. Phys. **73**, 6760 (1993).
- ⁶⁴B. Sadeh, M. Doi, T. Shimizu, and M. J. Matsui, J. Magn. Soc. Jpn. **24**, 511 (2000).
- ⁶⁵T. Yu, Z. X. Shen, W. S. Toh, J. M. Xue, and J. Wang, J. Appl. Phys. **94**, 618 (2003).
- ⁶⁶K. K. Nanda, A. Maisels, F. E. Kruis, H. Fissan, and S. Stappert, Phys. Rev. Lett. **91**, 106102 (2003).
- ⁶⁷V. P. Skripov, V. Koverda, and V. N. Skokov, Phys. Status Solidi A **66**, 109 (1981); H. Saka, Y. Nishikawa, and T. Imura, Philos. Mag. A **57**, 859 (1983).
- ⁶⁸J. Zhong, L. H. Zhang, Z. H. Jin, M. L. Sui, and K. Lu, Adv. Mater. (Weinheim, Ger.) **49**, 2897 (2001).
- ⁶⁹H. W. Sheng, G. Ren, L. M. Peng, Z. Q. Hu, and K. Lu, Philos.

- Mag. Lett. **73**, 179 (1996); L. Gråbaek, J. Bohr, E. Johnson, A. Johansen, L. Sarholt-Kristensen, and H. H. Andersen, Phys. Rev. Lett. **64**, 934 (1990); L. Zhang, Z. H. Jin, L. H. Zhang, M. L. Sui, and K. Lu, *ibid.* **85**, 1484 (2000); K. Chattopadhyay and R. Goswami, Prog. Mater. Sci. **42**, 287 (1997).
- ⁷⁰L. Lu, R. Schwaiger, Z. W. Shan, M. Dao, K. Lu, and S. Suresh, Adv. Mater. (Weinheim, Ger.) **53**, 2169 (2005).
- ⁷¹S. Veprek, M. G. J. Veprek-Heijman, P. Karvankova, and J. Prochazka, Thin Solid Films **476**, 1 (2005).
- ⁷²S. G. Srinivasan, X. Z. Liao, M. I. Baskes, R. J. McCabe, Y. H. Zhao, and Y. T. Zhu, Phys. Rev. Lett. **94**, 125502 (2005).
- ⁷³S. Ogata, J. Li, and S. Yip, Science **298**, 807 (2002).
- ⁷⁴G. H. Lu, S. Deng, T. Wang, M. Kohyama, and R. Yamamoto, Phys. Rev. B **69**, 134106 (2004).
- ⁷⁵K. Carling, G. Wahnstrom, T. R. Mattsson, A. E. Mattsson, N. Sandberg, and G. Grimvall, Phys. Rev. Lett. **85**, 3862 (2000).
- ⁷⁶C. Q. Sun, H. L. Bai, B. K. Tay, S. Li, and E. Y. Jiang, J. Phys. Chem. B **107**, 7544 (2003).
- ⁷⁷C. N. R. Rao, G. U. Kulkarni, P. J. Thomas, and P. P. Edwards, Chem.-Eur. J. **8**, 29 (2002).
- ⁷⁸It is interesting to note that only stable odd-layered films could form when the film is thinner than 22 monolayers. The stable odd-layered films are associated with monotonic a T_C drop and a gradual positive DOS shift with decreasing the number of atomic layers. It is anticipated that T_C would fluctuate up while remaining the general trend of T_C change with an association positive DOS shift for the rough thinner films.
- ⁷⁹Y. Hu, O. K. Tan, W. Cao, and W. Zhu, IEEE Sens. J. **5**, 825 (2005).
- ⁸⁰M. K. Zayed and H. E. Elsayed-Ali, Phys. Rev. B **72**, 205426 (2005).
- ⁸¹Q. Jiang and F. G. Shi, J. Mater. Sci. Technol. **14**, 171 (1998).
- ⁸²M. L. Alymov, E. I. Maltina, and Y. N. Stepanov, Nanostruct. Mater. **4**, 737 (1994).
- ⁸³H. Röder, E. Hahn, H. Brune, J. P. Bucher, and K. Kern, Nature (London) **366**, 141 (1993).